

Research Article

# Autoregulation of the MET receptor tyrosine kinase by its intracellular juxtamembrane domain

Edmond M. Linossi<sup>1</sup>, Carla A. Espinoza<sup>1</sup>, Gabriella O. Estevam<sup>2</sup>, James S. Fraser<sup>2,3</sup> and Natalia Jura<sup>1,3,4</sup> 

<sup>1</sup>Cardiovascular Research Institute, University of California San Francisco, San Francisco, CA, 94158, U.S.A.; <sup>2</sup>Department of Bioengineering and Therapeutic Sciences, University of California San Francisco, San Francisco, CA, 94158, U.S.A.; <sup>3</sup>Quantitative Biosciences Institute, University of California San Francisco, San Francisco, CA, 94158, USA; <sup>4</sup>Department of Cellular and Molecular Pharmacology, University of California San Francisco, San Francisco, CA, 94158, U.S.A.

Correspondence: Natalia Jura (natalia.jura@ucsf.edu)



Receptor tyrosine kinases (RTKs) are single-pass transmembrane receptors whose activation is tightly regulated by intra-domain interactions within both their extracellular and intracellular regions. The intracellular juxtamembrane (JM) domain, which links the transmembrane and kinase domains (KDs), often plays a critical role in modulating kinase activity. The MET receptor, activated by hepatocyte growth factor, requires precise regulation to support normal development and wound healing but becomes a potent oncogene when overexpressed or mutated. A common oncogenic lesion in MET, caused by exon 14 skipping, leads to partial deletion of its unusually long intracellular JM domain and is frequently detected in non-small cell lung cancer, as well as pancreatic, liver, and brain cancers. Despite its length and abundance of post-translational modifications, the functional role of the MET JM domain has remained poorly understood. We have uncovered that this segment regulates the kinetics of MET kinase activation. Specifically, we found that a membrane-proximal, N-terminal region of the JM domain accelerates activation loop phosphorylation, promoting kinase transition to an active state. This regulation does not depend on the oligomeric state of MET but likely acts allosterically to enhance autophosphorylation of the KD. Notably, this function is absent from the closely related MST1R/RON RTK, suggesting it is a unique feature of the MET receptor. Together, these findings uncover a previously unrecognized layer of MET regulation with potential implications for the development of selective therapies targeting MET-driven cancers.

## Introduction

Single-pass transmembrane receptor tyrosine kinases (RTKs) lie at the apex many of cellular signaling cascades. Binding of cognate growth factors to the extracellular domains induces RTK multimerization, or reorganization of existing receptor dimers, which in turn activates the intracellular tyrosine kinase domains (KDs) [1]. The activated KDs then proceed to phosphorylate tyrosine residues in receptor intracellular domains, which recruit signaling molecules that frequently also undergo phosphorylation, triggering a spectrum of downstream signaling cascades [2]. These include cellular motility, differentiation, and proliferation pathways, among others. The MET receptor, an RTK activated by the hepatocyte growth factor (HGF), plays a central role in regulating cell motility and proliferation [3–5]. MET signaling is essential for normal development in multicellular organisms and contributes to wound healing and tissue remodeling in adults [6,7]. A growing body of evidence also points to key roles of MET in immune and neuronal cell functions [8–10]. Aberrant activation of MET via gene amplification or mutations is a prominent feature of multiple human cancers [11,12].

MET contains a canonical tyrosine KD, composed of an N-lobe and a C-lobe with the catalytic active site located in between [13]. Multiple crystal structures of the MET KD and *in vitro* enzymatic studies have outlined the key steps of MET kinase activation [14]. In the inactive state, MET adopts a Src/Cyclin-Dependent Kinase (CDK)-like inactive conformation in which helix  $\alpha$ C is swung away from the active site and the activation loop adopts a short helical fold blocking substrate access. Sequential phosphorylation of the activation loop tyrosines in MET (Y1234 and Y1235) is key to the release of this autoinhibition, leading to the extension of the activation loop and enabling substrate binding [13,15–18]. This step also allows rotation of helix  $\alpha$ C towards the active site, establishing an essential Lys–Glu salt bridge (K1110 and E1127 in MET) that co-ordinates ATP for hydrolysis. In that way, MET follows a mechanism shared by other

Received: 10 August 2025  
Revised: 19 November 2025  
Accepted: 22 November 2025

Version of Record  
Published: 11 December 2025

RTKs, including insulin receptor (IR), platelet-derived growth factor receptor (PDGFR), FMS-like tyrosine kinase 3 (FLT3), and c-KIT, that rely on activation loop transphosphorylation for activity [19,20].

Additional regulatory mechanisms that maintain MET kinase in its autoinhibited state have been identified, with many of them compromised by mutations in cancer. For example, residues Y1230 and D1228 in the activation loop, and C-lobe residues F1200 and L1195, help stabilize the inactive conformation of the activation loop, and their mutation likely contributes to the disruption of the autoinhibitory tether [13,17]. Somewhat unexpectedly, these mutations often fail to induce constitutive receptor signaling and instead, they retain MET dependence on HGF binding for activation, even in an oncogenic setting [21–24]. Characterization of these mutations *in vitro* using the recombinant MET KD revealed that they accelerate kinase activation without altering the maximal catalytic rate of the enzyme [25]. These findings suggest that lowering the activation barrier for kinase activation alone is sufficient to drive oncogenic signaling, underscoring the importance of built-in autoinhibitory mechanisms in preventing untimely MET signaling.

One of the most common MET oncogenic mutations, occurring in approximately 5% of non-small cell lung cancer, falls outside of the KD and results in skipping of exon 14, which encodes the N-terminal half of the MET intracellular juxtamembrane (JM) domain [26–29]. This disease mutation underscores the potential importance of the JM domain, which connects the KD to the transmembrane domain, in MET regulation. In many RTKs, JM domains serve as central regulatory elements controlling kinase activity [30]. For example, in the inactive PDGFR, c-KIT, FLT3, and erythropoietin-producing human hepatocellular (Eph) receptors, the JM domain is directly tethered to the KD, restricting rotation of helix  $\alpha$ C [31–34]. This autoinhibitory mechanism is released by JM domain phosphorylation during activation of each of these receptors. In the human epidermal growth factor receptors (EGFRs/HERs), the JM domain does not seem to play a critical inhibitory role, but it is essential for kinase dimerization and allosteric control of kinase activation upon growth factor stimulation [35,36]. In the IR, which is a constitutive dimer, the JM domain switches from an inhibitory segment to an activating one upon IR stimulation [37–39]. By comparison, the role of the JM domain in the regulation of MET kinase activity remains poorly characterized.

In MET, the JM domain is substantially longer than in other RTKs: 92 residues in human MET (amino acids: 956–1048) compared with the typical ~10–50 amino acid length [30]. While a direct role of the JM domain in regulating MET kinase activity has not been established, specific residues within this region have been shown to contribute to negative feedback regulation of MET receptor signaling. Phosphorylation of Y1003 results in recruitment of the c-Cbl E3 ligase followed by ubiquitination and lysosomal degradation of MET [40,41]. Phosphorylation of S985 by Protein Kinase C (PKC) also negatively regulates MET, although the underlying mechanism remains unknown [42,43]. Under cellular stress, the MET JM domain can be cleaved by caspases at D1000 to release an intracellular MET fragment that promotes pro-apoptotic signaling [44–46]. Oncogenic exon 14 skipping mutations, which result in an in-frame deletion of residues 963–1009, eliminate all of these regulatory sites, complicating understanding how the JM domain contributes to MET-driven oncogenesis [47]. Elucidating the mechanisms by which the JM domain regulates MET kinase activity is therefore critical for understanding both its physiological and pathological roles.

In this study, we have investigated the direct role of the JM domain in regulation of MET kinase activity using purified proteins *in vitro*. Our findings reveal that the JM domain accelerates the autophosphorylation reaction required for full MET kinase activity and that this activity maps to the membrane-proximal, N-terminal region of the JM domain that largely overlaps with exon 14-encoded sequence. In contrast with other RTKs, the activating effect of the JM domain is not exerted by promoting kinase oligomerization but appears to entail allosteric regulation of the KD. Moreover, this mechanism does not rely on the Y1003 or S985 sites, suggesting that the activating role of the JM domain is distinct from its previously known regulatory functions in MET signaling. We also demonstrate that the activity of the KD of RON, a closely related MET ortholog, is not directly regulated by the JM domain, suggesting that MET employs a distinct, JM-driven mechanism for positive kinase regulation within the RTK family.

## Results

### The juxtamembrane region accelerates MET autophosphorylation

We investigated if the activity of the recombinant MET KD *in vitro* is modulated by the presence of the JM domain (residues K956–Q1048) (Figure 1A). We also looked if the presence of the short C-terminal

tail (C-tail) in MET, which encompasses residues G1346–S1390 (Figure 1A), contributes to potential JM domain-dependent regulation. A series of recombinant MET intracellular constructs were generated to include or omit the JM domain or C-tail: the full intracellular domain (ICD) including the C-tail (ICD: residues K956–S1390) or without the C-tail (ICD<sup>ΔC-tail</sup>: residues K956–G1346), the KD with the C-tail (KD: residues Q1048–S1390) or without the C-tail (KD<sup>ΔC-tail</sup>: residues Q1048–G1346). All constructs were expressed in insect cells, purified, and subject to dephosphorylation by lambda protein phosphatase to remove any tyrosine, serine, or threonine phosphorylation that could potentially elevate basal kinase activity. Kinase activity of all constructs was monitored in the absence or presence of a generic poly (Glu:Tyr) 4:1 substrate (hereafter referred to as ‘substrate’) using a coupled kinase assay [35,48] to evaluate autophosphorylation and substrate-directed MET activity.

The enzymatic activity of the KD displayed biphasic behavior during both autophosphorylation and substrate phosphorylation reactions, characterized by a slow initial rate followed by a faster rate, which we refer to as the ‘late’ rate (Figure 1B & C). Although the ICD and KD late rates were comparable, we observed that the presence of the JM domain led to acceleration of both MET kinase autophosphorylation and substrate phosphorylation. We consistently measured a ~4.5-fold faster autophosphorylation rate  $k_{\text{cat}}$  of the ICD compared with the KD ( $0.466 \pm 0.036 \text{ s}^{-1}$  compared with  $0.104 \pm 0.023 \text{ s}^{-1}$ , respectively) (Figure 1B). This difference in activity was further amplified (~9-fold faster) in the presence of the substrate (KD  $k_{\text{cat}} = 0.168 \pm 0.019 \text{ s}^{-1}$  compared with  $1.546 \pm 0.172 \text{ s}^{-1}$  for ICD) (Figure 1C). These results show that the JM domain accelerates the kinetics of activation without altering the enzyme’s maximal catalytic rate.

Biphasic activation of dephosphorylated KD was previously reported [49], with a transition between a slow initial rate and a faster late rate attributed to autophosphorylation of the MET activation loop on tyrosines Y1234 and Y1235. To investigate if KD and ICD exhibit different kinetics of activation loop phosphorylation, we dephosphorylated these constructs followed by incubation with ATP and MgCl<sub>2</sub> and monitored the phosphorylation of the activation loop tyrosines Y1234 and Y1235, as well as the C-tail tyrosine Y1235, over time by Western blot. Compared with the ICD, the KD exhibited a substantially slower rate of phosphorylation for both activation loop and C-tail sites (Figure 1D & E). These results show that the observed slower catalytic rate of the KD in the absence of the JM domain is due to delayed activation loop phosphorylation. If this is indeed the mechanism, we hypothesized that the KD construct in which the activation loop is fully phosphorylated prior to kinase activity measurements would not exhibit biphasic activation and have a comparable catalytic rate to ICD. To test this, the ICD and KD constructs were pre-incubated with ATP and MgCl<sub>2</sub> prior to the kinase assay. Under these conditions, the KD activation curve was no longer biphasic, and the catalytic rates of KD and ICD were comparable in the presence or absence of the substrate (Figure 1F–H). These results further support our conclusion that the JM domain augments MET kinase autophosphorylation, accelerating the initial rate of its activation.

The presence of the C-tail did not change the existing differences between initial rates of the KD and ICD constructs: the rate of MET ICD<sup>ΔC-tail</sup> was significantly faster compared with the MET KD<sup>ΔC-tail</sup> for both autophosphorylation and substrate-dependent activity (Supplementary Figure S1A&B). Removal of the C-tail from the ICD resulted in a small increase in catalytic rate relative to the construct containing the intact C-tail (~1.7-fold increase), pointing to a minor but reproducible negative regulation of the full ICD by the C-tail. Previous studies reported enhanced MET receptor activation in cells upon C-tail removal [50,51], and our findings with purified protein suggest this results from direct inhibition of the KD by the C-tail. Nevertheless, the mechanisms by which the JM domain and C-tail regulate MET kinase activity appear to be independent, as the presence of the JM domain accelerated initial rates under all conditions.

## ***In silico* sequence and structural analysis of the MET JM**

To investigate the mechanism for the potentiating effect of the JM domain on kinase activation, we performed an *in silico* analysis of its sequence conservation and potential secondary structural elements. In these predictions, we included the most C-terminal region of the JM domain (residues 1049–1070), which includes a short helix that is observed in all MET KD crystal structures and is likely integral to the KD fold [13]. We recently denoted this region as helix α<sub>JM</sub> [52]. The remaining MET JM domain encodes 92 amino acids (residues 956–1048) and has never been structurally characterized. For the purposes of the analysis, we divided this region into two segments: JM1 and JM2 (Figure 2A). The N-terminal segment (residues K956–D1010), designated as JM1, includes a short poly-basic sequence (residues K956–K962), predicted to bind the negatively charged lipids at the inner leaflet of the plasma membrane [53], and the region encoded by exon 14 (residues D963–E1009). The JM1 also includes two regulatory phosphorylation sites, a c-Cbl

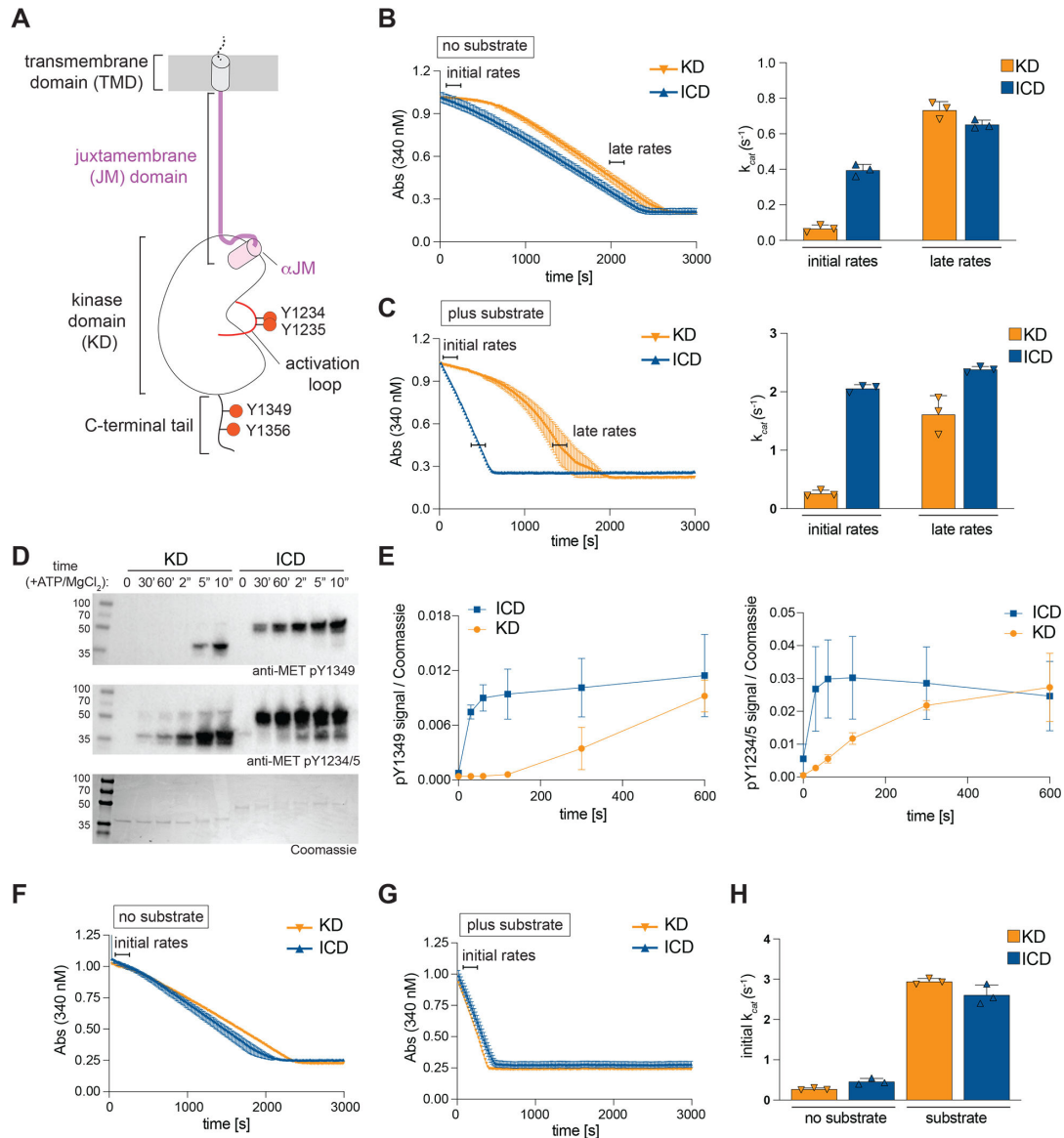


**Figure 1: The intracellular juxtamembrane domain accelerates MET kinase domain activation.**

(A) Schematic representation of the MET receptor intracellular and transmembrane domains. The extracellular ligand-binding region of MET is not shown. Regulatory phosphorylation sites in the activation loop and in the C-terminal tail are marked. (B–C) On the left, representative traces from the coupled kinase assay depict ATP consumption over time for the dephosphorylated kinase domain (KD) and full intracellular domain (ICD). The indicated regions used to calculate initial and late catalytic rates are marked by horizontal lines, and the rates are plotted in bar graphs on the right (triplicate data from one representative experiment). Measurements were conducted without the poly (Glu:Tyr) 4:1 substrate and correspond to KD autophosphorylation (B) or in the presence of a substrate (C). (D) Western blot analysis of KD and ICD autophosphorylation reaction using phospho-specific antibodies (specified below each blot). Coomassie staining was used to verify protein levels in all samples. (E) Quantification of the phosphorylated MET signal (Western) relative to total MET protein (Coomassie) for each site from three independent experiments. (F–G) Representative traces from the coupled kinase assay for the phosphorylated KD and ICD constructs, obtained in the absence (F) or presence of the substrate (G). (H) The calculated catalytic rates from triplicate measurements for representative experiments are shown in (F–G). Error bars represent standard deviation (SD). Supplementary Table S1 summarizes average values for each kinase assay from independent experiments.

recruitment site (Y1003) [40] and the PKC substrate residue S985 [43]. The C-terminal segment (residues D1010–Q1048) was designated as JM2 (Figure 2A).

We assessed sequence conservation of the MET JM domain using Aminode [54], which determines evolutionary constrained regions (ECRs) that represent contiguous sections of higher amino acid sequence conservation with respect to phylogenetic distance between different MET orthologs (Figure 2B). This analysis showed that the JM domain contains two ECRs: the poly-basic region that directly follows the transmembrane helix and a portion of JM1 (residues V975–D1010), which includes most of the

exon 14 coding region (Figure 2B). Conversely, the JM2 segment displayed lower evolutionary sequence conservation and a higher relative substitution score. Sequence alignment of MET orthologs also highlighted higher conservation of sequence and length across the JM1 segment compared with JM2 (Figure 2E; Supplementary Figure S2 displays sequence conservation across all orthologs). Additionally, phosphorylation sites within the JM domain, as annotated in the PhosphoSitePlus database [55], are predominantly clustered in the JM1 region (Figure 2E). Although the entire JM domain is predicted to be largely disordered (Figure 2C), both the Jpred secondary structure prediction tool [56] and AlphaFold3 [57] predict an isolated, short  $\alpha$  helix in the JM1 segment (Jpred: residues P978–S985; AlphaFold3: residues P978–S990) that has not been previously described (Figure 2D & E). Collectively, these analyses highlight that the JM1 segment of the MET JM domain is highly conserved, has evolved as a platform for post-translational modifications, and contains a region with a propensity to adopt a short helix. Together, these features point to JM1 as a region with the potential to act as a regulatory control site.

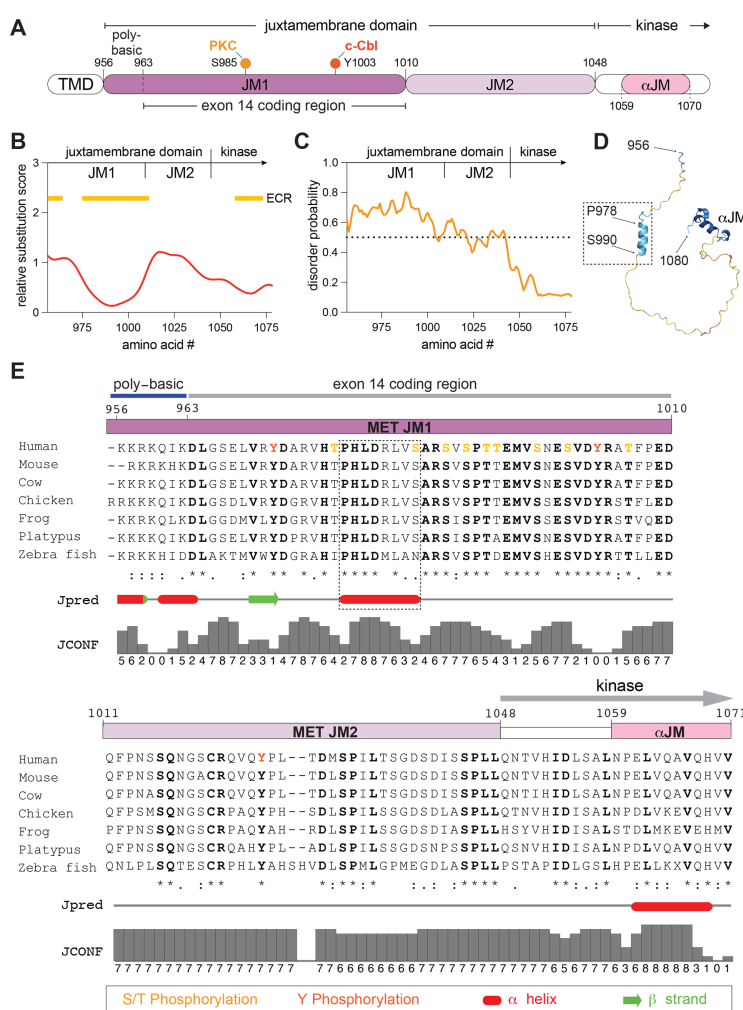


**Figure 2: Evolutionarily conserved features of the MET juxtamembrane domain.**

(A) Linear domain schematic of the MET intracellular fragment with key regions and amino acid numbers annotated. Key regulatory phospho-sites are indicated for reference: S985, which is phosphorylated by PKC, and Y1003, which recruits c-Cbl when phosphorylated. TMD stands for the transmembrane domain. (B) Conservation of the MET JM sequence was assessed using the Aminode algorithm. Values on Y-axis represent the relative substitution score for each amino acid number, with higher numbers indicating less sequence conservation. Yellow bars mark evolutionary conserved regions (ECRs) within the JM. (C) Disorder prediction for the MET JM using the IUPred2A algorithm. Dotted line indicates the order-disorder threshold; higher values reflect greater disorder. N-terminal region of the kinase domain fold is included for comparison. (D) AlphaFold3 model of the MET JM domain, colored by pLDDT (predicted local distance difference test) confidence scores. The location of the predicted N-terminal JM helix, the helix  $\alpha$ JM, and the boundary residues of the N- and C-terminal JM residues are annotated. (E) JM domain sequence alignment of selected MET orthologs is shown with subdomain regions annotated as in (A). Known phosphorylation sites are marked in red or orange. Dotted box marks the predicted N-terminal JM helix. Relative secondary structure predictions (marked red for  $\alpha$  helix and green for  $\beta$  sheet) and the corresponding confidence scores are shown below the sequence alignment.

## The JM1 segment is responsible for accelerated kinase activation

To investigate which region of the JM domain is responsible for accelerating kinase activation measured for ICD (Figure 1B and C), we expressed and purified ICD variants in which either JM1 (ICD<sup>ΔJM1</sup>) or JM2 (ICD<sup>ΔJM2</sup>) was deleted (Figure 3A). We also generated a construct in which JM2 was replaced with a repeating Gly-Ser linker of equal length (ICD<sup>JM2=GSL</sup>) to account for any steric effects resulting from fusing JM1 directly to the KD (Figure 3A). Analysis of the autophosphorylation activity of these constructs revealed that deletion of the JM2 segment had no effect on the initial rates relative to the full ICD, whereas deletion of the JM1 segment abolished the accelerating effect of the JM domain on kinase autophosphorylation activity (Figure 3B). The initial activation rate of the ICD<sup>ΔJM1</sup> was equivalent to the KD alone and displayed biphasic activation kinetics (Figure 3B). The JM1 segment was also responsible for the accelerated substrate-dependent kinase rate (Figure 3C). Curiously, while deletion of JM2 did not alter kinase activity, when this segment was replaced with a flexible GS-linker, autophosphorylation and substrate-dependent rates were slightly elevated (~1.5-fold) compared with the wild type ICD (Figure 3B & C). This suggests that JM1-mediated kinase activation may be regulated by both spatial distance from the kinase and the JM2-encoded sequence.

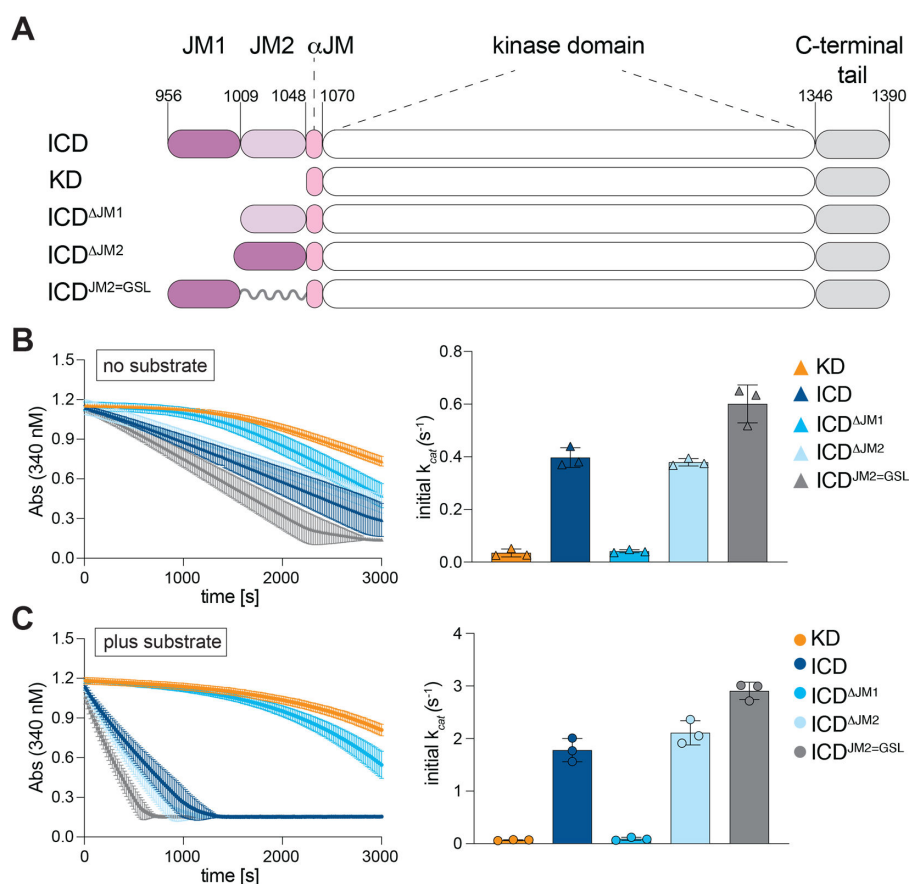


**Figure 3: The JM1 region is responsible for accelerated MET kinase activation.**

(A) Schematic depiction of the MET JM domain constructs. Glycine-Serine linker (GSL) (B-C) Representative traces from the coupled kinase assay for the dephosphorylated constructs, obtained in the absence (B) or presence of substrate (C). Bar graphs on the right show the calculated catalytic rates from triplicate measurements for a representative experiment. Error bars represent standard deviation (SD). Supplementary Table S1 summarizes average values for each kinase assay from independent experiments.

## Known phosphorylation sites do not directly contribute to the activating effect of the JM1 region

Numerous RTKs are regulated by phosphorylation of tyrosine residues in their JM domains, which frequently serves to release autoinhibitory interactions imposed on the KD [30]. We observed that the c-Cbl-binding site Y1003 is autophosphorylated by MET *in vitro* using a phospho-specific antibody (Supplementary Figure 3A), suggesting that this event may contribute to the accelerated activation in our assays. We investigated whether preventing phosphorylation of this site would modulate the potentiating effect of JM1 on kinase activity by generating a non-phosphorylatable Y1003F mutant. We also looked at the effect of mutation of another known JM1 phosphorylation site, the PKC site S985, by generating its non-phosphorylatable variant (S985A) and a phospho-mimetic (S985E). All three mutant ICD constructs exhibited activity equivalent to the wild type ICD (Supplementary Figure 3B–D), thus arguing against the role of these post-translational modifications in direct regulation of JM1-dependent kinase activation.

## The MET JM domain acts independently of kinase multimerization

One possible mechanism by which JM1 accelerates kinase activation is through promoting multimerization of the intracellular domain, thereby facilitating more efficient trans-phosphorylation of the kinase activation loop. We measured the oligomeric state of the KD and ICD constructs using size exclusion chromatography coupled with multi-angle light scattering (SEC-MALS). The ICD and KD both migrated as single peaks with calculated molecular weights corresponding to their respective monomeric states (Figure 4A). Notably, the SEC-MALS analysis was conducted at a protein concentration of 20  $\mu$ M, 100-fold higher than that in the coupled kinase assay, strongly arguing against JM1-mediated oligomerization as a mechanism of kinase activation.

Ligand-mediated dimerization is a key step in MET receptor activation, promoting kinase autophosphorylation. Since the isolated ICD is monomeric in our assays, we tested whether the accelerating effect of the JM1 segment is retained when the MET KD is locked in a constitutive dimer. To engineer such dimers, we utilized the gene-fusion product translocated promoter region (TPR)-MET, a rare occurring oncogene, in which a coiled-coil dimerization motif of TPR protein is fused in frame with part of the intracellular region of MET (residues D1010-S1390) [3,58]. This constitutively dimerized MET fragment has been utilized extensively to understand growth factor-independent MET signaling in cells [59–62]. Because the exon 14-coding region, which encompasses a majority of the JM1 segment, is absent from TPR-MET, we generated a variant in which it is restored (residues D963-E1009, denoted as TPR-MET<sup>+exon14</sup>) (Figure 4B). All TPR-MET variants were expressed and purified from insect cells followed by lambda phosphatase-mediated dephosphorylation. Surprisingly, the autophosphorylation and substrate-dependent catalytic rate of TPR-MET were only slightly elevated compared with the monomeric KD, indicating that TPR-mediated dimerization of the MET KDs does not significantly accelerate their activation (Figure 4C–D). The activity of dimerized TPR-MET was also significantly lower than that of monomeric ICD, supporting the conclusion that the JM domain's potentiating effect on kinase activity is unlikely to stem from enhanced dimerization. Furthermore, the region encoded by exon 14 elevated activity of the dimerized KD (TPR-MET vs. TPR-MET<sup>+exon14</sup>) (Figure 4C–D), suggesting that the JM1 domain might be activating the kinase via an allosteric mechanism such as direct binding. The lower observed activating effect of the JM in the TPR-MET context, relative to the monomeric ICD, may indicate that TPR-mediated dimer restrains or limits the ability of the JM domain to engage the associated KDs. The TPR-MET<sup>+exon14</sup> construct also lacks the short poly-basic region (residues K956-D963) present in the full MET ICD; thus, it is also possible that this region provides an additional activating signal.

We used an ADP-Glo assay as an alternative activity assay to corroborate our measurements obtained using the TPR fusion constructs. Relative kinase activity was determined in the presence of saturating concentrations of ATP/MgCl<sub>2</sub> and in the presence or absence of the substrate after a 60-min incubation time. Consistent with the coupled kinase assay results, the ICD had higher activity relative to KD (~2.8-fold) (Figure 4E). In the ADP-Glo assay, TPR-MET exhibited a measurable (~1.8-fold) increase in autophosphorylation compared with the KD (Figure 4E), and inclusion of the exon 14-coding region further increased activity (~2.5-fold over KD) (Figure 4E). Similarly, in the presence of the substrate, the exon 14-coding region further accelerated kinase activity of TPR-MET (Figure 4E). While differences in the assay format and associated activity readout between the ADP-Glo (endpoint, total ATP hydrolysis) and coupled kinase assay (initial ATP hydrolysis rate) may influence apparent activity differences between

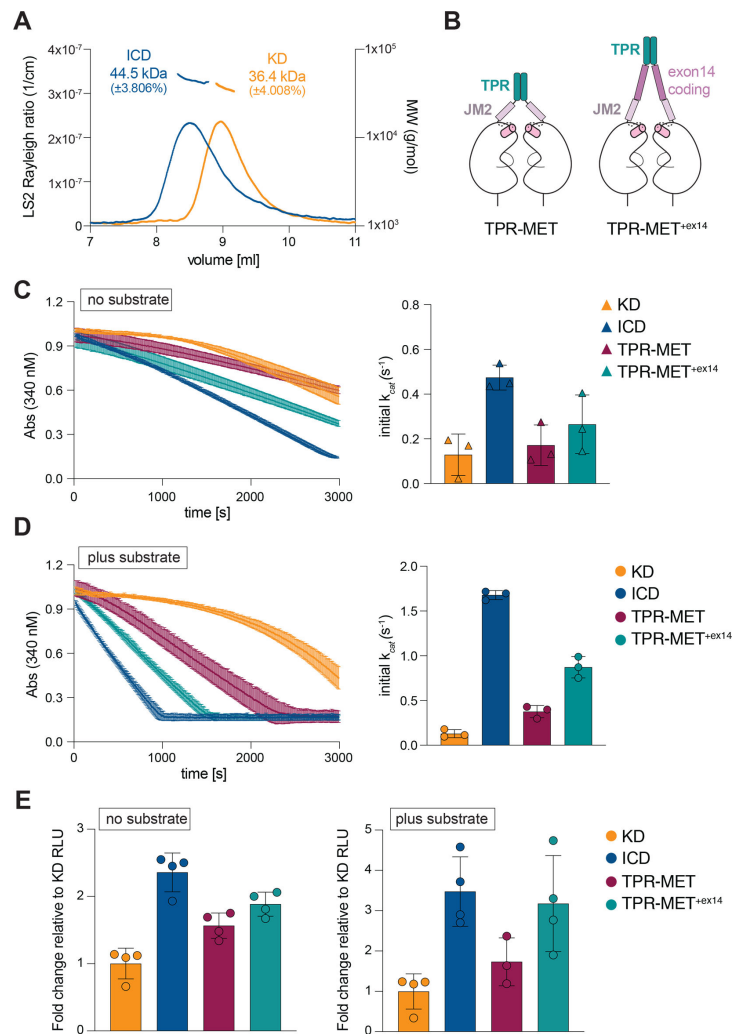


**Figure 4: The juxtamembrane domain activates MET independently of dimerization.**

(A) Size-exclusion chromatography coupled with multi-angle light scattering (SEC-MALS) analysis of the dephosphorylated KD and ICD. Elution volume from the size exclusion column is plotted on the x-axis. The left y-axis shows the light-scattering signal. Calculated molecular weights (MW) are indicated above the elution peaks, with their distribution shown on the right y-axis. (B) Schematic depiction of the dimeric MET constructs engineered via fusion of the translocated promoter region (TPR). (C–D) Representative traces from the coupled kinase assay for the indicated dephosphorylated MET constructs, obtained in the absence (C) or presence (D) of substrate. Bar graphs on the right show the calculated catalytic rates from triplicate measurements for a representative experiment. Error bars represent standard deviation (SD). (E) ADP-Glo activity measurements for the indicated proteins are shown as fold change in relative luminescence units (RLUs), normalized to the activity of KD measured in the absence (left) or presence (right) of substrate. Supplementary Table S2 summarizes average values for each ADP-Glo assay from independent experiments.

the constructs, this analysis collectively highlights that the JM1 segment accelerates MET kinase activation of the monomeric KD, without promoting its dimerization.

## The JM regulatory role is not conserved in RON

MET has only one close homolog, called *recepteur d'origine nantais* (RON) or macrophage-stimulating protein receptor (MST1R). RON also contains an elongated JM domain (residues 983–1074), although it shares only modest sequence homology with MET (24% amino acid identity) (Figure 5A). Previous studies identified two putative regulatory regions within the RON JM domain. The first corresponds to a stretch of 27 amino acids (P1009–V1035), designated as JMB, which inhibits RON activation in cells [63,64]. The second is a short stretch of acidic residues (EDE, E1044–E1046), whose mutation to alanine residues increases RON activation in cells [64]. *In silico* analysis of the human RON JM domain using Aminode revealed an ECR corresponding to the JMB segment, while the remainder of the JM domain showed a relatively high substitution score across RON orthologs (Figure 5B). AlphaFold3 predicted a short  $\alpha$  helix



c-Cbl and PKC, to date, no direct role for this domain in controlling kinase activity has been described. Here we report the first direct analysis of the role of the MET JM domain in activation of the KD *in vitro* and show that the N-terminal JM region, denoted by us as JM1, substantially increases initial catalytic rate of the MET kinase by accelerating autophosphorylation kinetics of the activation loop tyrosines Y1234 and Y1235. We found that once the activation loop tyrosines in MET are phosphorylated, the JM domain does not further elevate kinase activity. Thus, the JM domain promotes the transition of the MET kinase from an inactive to an active state via accelerating kinase autophosphorylation.

The activating effect of the JM domain maps to its N-terminal 46 amino acids (the JM1 segment), as only the removal of this segment prevented the accelerated activation kinetics in our studies. Our analysis shows that within the JM domain, the JM1 region is most highly conserved. It contains nine serine/threonine and two tyrosine residues known to be phosphorylated, including regulatory sites for c-Cbl recruitment (Y1003) and PKC-mediated down-regulation (S985), indicating this region is important for MET receptor regulation. Our computational analysis points to a high likelihood of an  $\alpha$  helix in the JM1 region, which encompasses S985. Although the contribution of the predicted  $\alpha$  helix to the activating function of the JM1 segment remains undefined, our results demonstrate that mutation of S985 does not alter this activity.

At present, we do not fully understand the mechanism by which the MET JM1 segment accelerates kinase autophosphorylation. In many RTKs, which harbor a short JM domain, extracellular domain dimerization and reorganization of the transmembrane helices help to bring the KDs into close proximity for their transactivation, and the JM domain often regulates this process. This is the case in EGFR, for example, in which the JM domain promotes kinase dimerization following growth factor stimulation [19,36]. However, the JM domain in MET presents a challenge for driving kinase proximity due to its 93 amino acid length, predicted largely unstructured nature, and the resulting high conformational flexibility. Consequently, we did not observe a measurable effect of the JM domain on MET kinase oligomerization, and the ICD construct remained monomeric far beyond the concentration range used in the kinase assays. Moreover, constitutive MET kinase dimerization in the TPR-MET construct led to only a modest increase in MET catalytic rate, whereas inclusion of the JM1 domain activating segment to this construct elevated kinase activity. Collectively, this suggests that the activating effect of the JM domain might be mediated through a direct interaction with the KD, which could either tether the kinases closer to the membrane or release kinase autoinhibition, thereby accelerating activation kinetics.

In support of the allosteric mechanism come our recent studies in which we conducted deep mutational scan analysis of the MET KD, in a TPR-MET context, and used MET receptor signaling-dependent BaF3 cell survival as a readout [52]. This analysis pointed to direct communication between the exon 14-coding region and the interface between helix  $\alpha$ C and  $\alpha$ JM within the MET KD. Specifically, we observed that mutation of the hydrophobic interface between helix  $\alpha$ C and  $\alpha$ JM helices resulted in loss-of-function variants, but only when the TPR-MET construct included the exon 14-coding region, hinting at a communication between these distant structural elements. The precise mechanism by which the helix  $\alpha$ C/ $\alpha$ JM interface regulates the MET signaling or activation has yet to be defined. Rotation of helix  $\alpha$ C is a critical step in the activation of many protein kinases, which have evolved diverse mechanisms to regulate it via direct interactions between regulatory elements and the helix  $\alpha$ C [19]. Whether the JM1 segment engages this interface to regulate the kinetics of MET kinase activation remains to be determined in future studies.

The JM-mediated effect that lowers the activation threshold required for efficient activation loop autophosphorylation and maximal catalytic activity resembles the effect observed with several oncogenic mutations in the MET KD. These mutations, including L1195V, D1228H, Y1230C, Y1235D, and M1250T, typically target the intramolecular autoinhibitory interactions within the MET KD [17,24,44]. Analogous to the effect of the JM domain we have observed here, analysis of these KD mutants *in vitro* showed accelerated autophosphorylation and initial catalytic rates of the MET kinase compared with its wild type counterpart, without an effect on maximal catalytic rate [25]. A similar phenomenon has been shown in cells in which the same mutations can lower the activation threshold required for receptor activation but often do not render MET ligand-independent or constitutively active [21–24,67]. This notion of lowering the activation threshold required for kinase activation, rather than resulting in constitutive activity, is also exemplified by recently described mutations in the MET kinase N-lobe identified in patients with hereditary papillary renal cell carcinoma [67]; the mutant receptors remain dependent on HGF activation to drive tumorigenesis.

An intriguing question is how the activating effect of the JM1 segment *in vitro* reported here can be reconciled with the pro-oncogenic effect of exon 14 skipping observed in patients, which effectively corresponds to the loss of the JM1 domain in MET. A recent study showed that oncogenic signaling by the exon 14 skipping mutant can be recapitulated by the Y1003F mutation, which prevents c-Cbl binding within the exon 14 region [47]. This suggests that exon 14 skipping exerts its oncogenic signaling primarily by slowing down MET down-regulation. This could indicate that slower MET activation kinetics, expected to result from loss of JM1, and prolonged signaling due to loss of c-Cbl binding may cooperate to disrupt intracellular receptor regulation, ultimately promoting cellular transformation. Similar to KD mutations, exon 14-skipped MET remains ligand-dependent in the absence of receptor overexpression, and cells harboring this variant show prolonged signaling upon HGF stimulation [68]. An alternative model that rationalizes why exon 14 skipping exerts a net activating effect on MET signaling assumes that shortening the JM domain brings the KDs into closer proximity to the plasma membrane, which serves as a hub for interactions of multiple signaling modules, including PI3K and AKT. Receptor dimerization, kinase activation, and recruitment of these signaling regulators may coalesce a more potent signaling hub to drive oncogenesis, despite a potential decrease in kinase activation kinetics. Refining the precise amino acid region within the JM1 domain that contributes to accelerated kinase activation observed *in vitro* will be essential to disentangle the relative contribution of JM1 in the full-length MET from both c-Cbl regulation and the broad effects observed from exon 14 skipping seen in cells.

In addition to the significant activating effect of the JM domain on MET kinase activity, our studies also reveal a modest inhibitory role of the MET C-tail. The MET C-tail region encodes two key tyrosine phosphorylation sites (Y1349 and Y1356), forming a so-called ‘bidentate’ motif, which is crucial for the recruitment of MET downstream adapters, including Grb2, PLC $\gamma$ , PI3K, and Gab1. While the C-terminal tyrosines are essential for MET signaling, previous studies have shown the C-tail may also inhibit MET prior to activation, as the catalytic activity of the MET receptor immunoprecipitated from cells is higher in the absence of the C-tail [51]. A crystal structure of the MET KD with a portion of the C-tail (residues G1346–K1360) depicts the tail, including the bidentate motif, as docked at the bottom of the MET kinase C-lobe, offering a potential mechanism for intramolecular autoinhibition [13]. The region, encompassing the F1341–Y1356 residues of MET, which includes the part of the folded kinase C-lobe, is also important for direct binding of the Gab1 adaptor protein [69]. The relative positioning of the C-tail may both reduce kinase activation, as observed here, and restrict adaptor access until this region is phosphorylated. Analysis of the related RON KD *in vitro* also revealed a direct regulation of its catalytic activity by the C-tail [70]. Mutation of the bidentate motif, also present in the RON C-tail, to phenylalanines similarly increased RON kinase activity, implicating their role in kinase autoinhibition [70]. Thus, MET and RON appear to utilize a similar regulatory mechanism involving their C-tails, which is likely relieved upon autophosphorylation of the key tyrosines in this region. In contrast, we show that RON kinase activity is largely unaffected by the JM domain, as its deletion did not alter activation kinetics of the RON kinase. Notably, the JM and C-tail regions appear to act independently in regulating MET kinase activity, as the JM domain substantially impacts catalytic activity regardless of the presence or absence of the C-tail.

Small-molecule inhibitors of MET have shown clinical efficacy in several human cancers, but resistance mutations often limit their durability [71–75]. Elucidating the mechanisms that regulate MET signaling is key to managing resistance and uncovering new therapeutic vulnerabilities. Our finding of the new role of the JM domain in the regulation of MET kinase adds to the emerging evidence that the MET JM domain functions as a multiplex platform for integrating both activating and inhibitory signals to control MET signaling. While further studies are needed to elucidate the mechanisms by which the JM domain activates MET kinase, our findings highlight the JM domain as a potential therapeutic target for inhibiting MET signaling. For example, small molecules that block JM1-like interactions with the KD could potentially attenuate activation while preserving c-Cbl-mediated down-regulation of MET.

## Experimental procedures

### Constructs

All MET, TPR-MET, and RON kinase constructs used in this study were cloned into a modified pFastBac (Thermo Fisher Scientific) plasmid including an N-terminal 10 $\times$  Histidine tag and Tobacco etch virus (TEV) cleavage sequence (SYHHHHHHHHHHHDYDIPTTENLYFQG). All point mutants were generated

using QuickChange mutagenesis (Agilent Technologies) following standard protocols. All construct boundaries are listed in Supplementary Table S3.

## Protein expression and purification

All MET and RON KD-containing proteins, including TPR-MET variants, were expressed and purified from Sf9 insect cells (Expression Systems) using the protocol detailed below. High titer baculovirus for each construct was generated using standard protocols of the Bac-to-Bac system (Thermo Fisher Scientific) and used to inoculate 1 l cultures ( $2 \times 10^6$  cells/ml, 27°C incubation, 110 rpm shaking) at a 1:40 ratio. Cultures were harvested 48–72 h later by centrifugation, and cell pellets were flash frozen and stored at –80°C. Pellets were thawed on ice in lysis buffer (50 mM HEPES, pH 8.0, 250 mM NaCl, 20 mM imidazole, 5 mM  $\beta$ -mercaptoethanol (BME), 10% glycerol (v/v), with the addition of cOmplete™ Mini, EDTA-free Protease Inhibitor Cocktail tablets (Roche) and DNase I (Roche). Resuspended pellets were lysed by homogenization with three passages through an EmulsiFlex-C5 (Avestin) at 10 Kpsi followed by ultracentrifugation at  $40,000 \times g$  for 1 h. Soluble proteins were filtered through 0.45  $\mu$ m filters prior to loading to HisTrap HP 1 ml or 5 ml columns (Cytiva). Bound proteins were extensively washed in nickel buffer A (20 mM HEPES, pH 8.0, 500 mM NaCl, 5% glycerol (v/v), 5 mM BME, and 20 mM Imidazole). Increasing concentrations of Nickel Buffer B (Nickel Buffer A with 500 mM Imidazole) up to 15% were used to further remove weakly bound proteins followed by a gradient elution from 15 to 100% Nickel Buffer B. Eluted proteins were monitored by SDS-PAGE followed by Coomassie staining, and fractions containing MET or RON were pooled, diluted 1:1 with Nickel Buffer A, and incubated overnight with TEV protease (1:50 TEV/protein) at 4°C without mixing. TEV-cleaved protein was re-run on a 1 ml or 5 ml column HisTrap HP, and the flow-through was collected, concentrated, and further purified on a S200 Increase 10/300 GL column (Cytiva) in SEC buffer [20 mM HEPES, pH 8.0, 250 mM NaCl, 2 mM [tris(2-carboxyethyl)phosphine] and 5% glycerol (v/v)]. Fractions containing pure MET or RON were pooled, concentrated using 30 kDa MWCO centrifuge filters (Amicon) to 0.5–4 mg/ml, flash frozen, and stored at –80°C until assayed. To generate dephosphorylated samples, proteins were incubated with Lambda Protein Phosphatase (NEB) and 10 mM  $MnCl_2$  at 18°C for 16–20 h. For phosphorylation, proteins were incubated with 2 mM ATP and 10 mM  $MgCl_2$  under the same conditions. After dephosphorylation or phosphorylation, all samples were subjected to SEC, concentrated, and stored as described above.

## Coupled kinase assay

Kinase activity was measured using a continuous spectrophotometric assay that couples NADH oxidation to ATP consumption [35,48]. All reactions were performed at 25°C in the presence of kinase reaction mixture (100 mM HEPES, pH 8.0, 10 mM  $MgCl_2$ , 1 mM PEP, 56 U/ml PK/LDH, 0.3 mg/ml NADH, and 2 mM ATP) in the presence or absence of 5 mg/ml poly (Glu:Tyr) 4:1 peptide (Sigma). Reactions were initiated by the addition of 0.2 mM recombinant kinase unless stated otherwise in the figure legends. The conversion of NADH to  $NAD^+$  was monitored by measuring the decrease in absorbance at 340 nm over time using a Biotek Synergy H1 multimode reader (Agilent). Reaction rates were derived from changes in absorbance over time [35], and calculated  $k_{cat}$   $s^{-1}$  values are quoted as mean  $\pm$  SEM. Initial reaction rates were determined between 30 and 300 s and late reaction rates between 340 nm values of 0.45 and 0.35. All kinase assays were performed with technical triplicates with at least two independent experiments using independently prepared protein. A summary of all measurements is provided in Supplementary Table S1. *P*-values shown in Supplementary Table S1 were calculated using Welch's t-test on independent experimental means.

## ADP-Glo kinase assay

Catalytic activity of MET and TPR-MET constructs was determined using the ADP-Glo kinase assay (Promega). Proteins were diluted to 0.2  $\mu$ M final concentration in 20  $\mu$ l reaction volume containing 2 mM ATP and 10 mM  $MgCl_2$  in the presence or absence of 5 mg/ml final poly (Glu:Tyr) 4:1 peptide. ADP production was monitored after 60 min at 24°C, following the manufacturer's recommendations, and luminescence was measured on a Biotek Synergy H1 multimode reader (Agilent). Preliminary experiments established that this concentration of MET and time point fall within the linear phase of the reaction. The measured relative luminescence units (RLUs) are represented as fold-change relative to the RLU values for the KD and are quoted as mean  $\pm$  SEM (Supplementary Table S2).

## Size exclusion chromatography-multi-angle scattering (SEC-MALS)

Dephosphorylated MET proteins (100  $\mu$ l of 20  $\mu$ M protein) were separated on a Shodex KW-802.5 column by High-Performance Liquid Chromatography (HPLC) with a UV detector (Shimadzu), connected with a miniDAWN MALS detector and an Optilab refractometer (Wyatt Technology) at 4°C. Molecular weight was determined using the Astra software package (Astra v8.3.0.132 Wyatt Technology).

## Western blot analysis of MET phosphorylation

To monitor MET autophosphorylation, dephosphorylated recombinant proteins were diluted to 1  $\mu$ M in SEC buffer, and an initial sample was taken (time 0) before adding 2 mM ATP and 10 mM MgCl<sub>2</sub>. Reactions were sampled at the indicated times and diluted 4-fold directly in Laemmli sample reducing buffer to stop the reaction. Samples were separated by SDS-PAGE, and gels were either stained with Coomassie for total MET quantification or transferred to nitrocellulose membranes for Western blot analysis. The following phospho-specific antibodies were used to detect phosphorylation of MET Y1349 in the C-tail (#3133, CST) and Y1234/Y1235 in the activation loop (#3077, CST), using enhanced chemiluminescence (Amersham) and a ChemiDoc MP Imaging System (Bio-Rad). Intensity of MET-specific phosphorylation levels was calculated relative to total MET protein detected by Coomassie staining and quantified using Image Lab software (v6.1, Bio-Rad). Western blot and Coomassie images from replicate experiments are included in Supplementary Data S1. Phosphorylation at MET Y1003 (#3135, CST) was also measured to confirm complete dephosphorylation of the recombinant MET protein (Supp Figure 3).

## *In silico* analysis of evolutionary sequence conservation

Human MET phosphorylation sites cited at least five times in prior publications or data sets were extracted from Phosphosite Plus [55]. Sequence conservation and evolutionary constrained regions were derived from Aminode [54] using standard parameters. Data were downloaded and reformatted in Prism (v10.4.1) to focus on the intracellular JM domain of MET and RON. Sequence conservation of MET was additionally assessed by sequence alignment of MET orthologs extracted from <https://www.ncbi.nlm.nih.gov/datasets/gene/4233/#orthologs>. Sequences were aligned using Clustal Omega [76], and a consensus sequence logo for the MET intracellular region is displayed in Supplementary Figure S2. Sequence alignment from selected species with gaps removed is shown in Figure 2E. Secondary structure prediction and protein folding analysis were performed using Jpred 4 [56] and the AlphaFold 3 server [57], respectively, using the intracellular JM regions of human MET (amino acids 956–1071) and human RON (amino acids 983–1074). AlphaFold3 models were analyzed in PyMOL (v.3.0.0, Schrödinger). Disorder prediction of the equivalent region of MET was assessed using the IUPred2A server [77].

## Data Availability

All data supporting the findings of this study are included in the article and its supplementary materials.

## Competing Interests

The authors declare that there are no competing interests associated with the manuscript.

## Open Access

This article has been published open access under our Subscribe to Open programme, made possible through the support of our subscribing institutions, learn more here: [https://portlandpress.com/pages/open\\_access\\_options\\_and\\_prices#conditional](https://portlandpress.com/pages/open_access_options_and_prices#conditional)

## CRedit Author Contribution

E.M. Linossi contributed to writing original draft, conceptualization, funding acquisition, writing review and editing, data curation, investigation, methodology, and formal analysis. C.A. Espinoza contributed to

conceptualization, writing review and editing, data curation, investigation, formal analysis, and methodology. G.O. Estevam contributed to conceptualization and writing review and editing. J.S. Fraser contributed to funding acquisition, supervision, and writing review and editing. N. Jura contributed to writing original draft, conceptualization, funding acquisition, supervision, investigation, and formal analysis.

## Abbreviations

BME,  $\beta$ -mercaptoethanol; CDK, Cyclin-dependent kinase; C-tail, C-terminal tail; ECR, evolutionary conserved region; EGFRs, epidermal growth factor receptors; Eph, erythropoietin-producing human hepatocellular; FLT3, FMS-like tyrosine kinase 3; HGF, hepatocyte growth factor; HPLC, High-Performance Liquid Chromatography; HPRC, hereditary papillary renal cell carcinoma; IR, insulin receptor; JM, juxtamembrane; KD, kinase domain; PDGFR, platelet-derived growth factor receptor; PKC, Protein Kinase C; RLU, relative luminescence units; RON, recepteur d'origine nantais; RTKs, receptor tyrosine kinases; SD, standard deviation; SEC-MALS, size exclusion chromatography coupled with multi-angle light scattering; TEV, Tobacco Etch Virus; TPR, translocated promoter region.

## References

- 1 Trenker, R. and Jura, N. (2020) Receptor tyrosine kinase activation: from the ligand perspective. *Curr. Opin. Cell Biol* **63**, 174–185 <https://doi.org/10.1016/j.ceb.2020.01.016> PMID: 32114309
- 2 Lemmon, M.A. and Schlessinger, J. (2010) Cell signaling by receptor tyrosine kinases. *Cell* **141**, 1117–1134 <https://doi.org/10.1016/j.cell.2010.06.011> PMID: 20602996
- 3 Cooper, C.S., Park, M., Blair, D.G., Tainsky, M.A., Huebner, K., Croce, C.M. et al. (1984) Molecular cloning of a new transforming gene from a chemically transformed human cell line. *Nature* **311**, 29–33 <https://doi.org/10.1038/311029a0>
- 4 Park, M., Dean, M., Kaul, K., Braun, M.J., Gonda, M.A. and Vande Woude, G. (1987) Sequence of MET protooncogene cDNA has features characteristic of the tyrosine kinase family of growth-factor receptors. *Proc. Natl. Acad. Sci. U.S.A.* **84**, 6379–6383 <https://doi.org/10.1073/pnas.84.18.6379> PMID: 2819873
- 5 Bottaro, D.P., Rubin, J.S., Faletto, D.L., Chan, A.M.-L., Kmieciak, T.E., Vande Woude, G.F. et al. (1991) Identification of the hepatocyte growth factor receptor as the *c-met* Proto-Oncogene Product. *Science* **251**, 802–804 <https://doi.org/10.1126/science.1846706>
- 6 Trusolino, L., Bertotti, A. and Comoglio, P.M. (2010) MET signalling: principles and functions in development, organ regeneration and cancer. *Nat. Rev. Mol. Cell Biol.* **11**, 834–848 <https://doi.org/10.1038/nrm3012> PMID: 21102609
- 7 Petrini, I. (2015) Biology of MET: a double life between normal tissue repair and tumor progression. *Ann. Transl. Med.* **3**, 82 <https://doi.org/10.3978/j.issn.2305-5839.2015.03.58> PMID: 25992381
- 8 Ilangumaran, S., Villalobos-Hernandez, A., Bobbala, D. and Ramanathan, S. (2016) The hepatocyte growth factor (hgf)-met receptor tyrosine kinase signaling pathway: diverse roles in modulating immune cell functions. *Cytokine* **82**, 125–139 <https://doi.org/10.1016/j.cyto.2015.12.013> PMID: 26822708
- 9 Hübel, J. and Hieronymus, T. (2015) HGF/Met-Signaling Contributes to Immune Regulation by Modulating Tolerogenic and Motogenic Properties of Dendritic Cells. *Biomedicines* **3**, 138–148 <https://doi.org/10.3390/biomedicines3010138> PMID: 28536404
- 10 Desole, C., Gallo, S., Vitacolonna, A., Montarolo, F., Bertolotto, A., Vivien, D. et al. (2021) HGF and MET: from brain development to neurological disorders. *Front. Cell Dev. Biol.* **9**, 683609 <https://doi.org/10.3389/fcell.2021.683609> PMID: 34179015
- 11 Sattler, M. and Salgia, R. (2025) The expanding role of the receptor tyrosine kinase MET as a therapeutic target in non-small cell lung cancer. *Cell Rep. Med.* **6**, 101983 <https://doi.org/10.1016/j.xcrm.2025.101983> PMID: 40020676
- 12 Comoglio, P.M., Trusolino, L. and Boccaccio, C. (2018) Known and novel roles of the MET oncogene in cancer: a coherent approach to targeted therapy. *Nat. Rev. Cancer* **18**, 341–358 <https://doi.org/10.1038/s41568-018-0002-y> PMID: 29674709
- 13 Schiering, N., Knapp, S., Marconi, M., Flocco, M.M., Cui, J., Perego, R. et al. (2003) Crystal structure of the tyrosine kinase domain of the hepatocyte growth factor receptor c-Met and its complex with the microbial alkaloid K-252a. *Proc. Natl. Acad. Sci. U.S.A.* **100**, 12654–12659 <https://doi.org/10.1073/pnas.1734128100> PMID: 14559966
- 14 Linossi, E.M., Estevam, G.O., Oshima, M., Fraser, J.S., Collisson, E.A. and Jura, N. (2021) State of the structure address on MET receptor activation by HGF. *Biochem. Soc. Trans.* **49**, 645–661 <https://doi.org/10.1042/BST20200394> PMID: 33860789
- 15 Chiara, F., Michieli, P., Pugliese, L. and Comoglio, P.M. (2003) Mutations in the met oncogene unveil a “dual switch” mechanism controlling tyrosine kinase activity. *J. Biol. Chem.* **278**, 29352–29358 <https://doi.org/10.1074/jbc.M302404200> PMID: 12746450
- 16 Cristiani, C., Rusconi, L., Perego, R., Schiering, N., Kalisz, H.M., Knapp, S. et al. (2005) Regulation of the wild-type and Y1235D mutant Met kinase activation. *Biochemistry* **44**, 14110–14119 <https://doi.org/10.1021/bi051242k> PMID: 16245927
- 17 Wang, W., Marimuthu, A., Tsai, J., Kumar, A., Krupka, H.I., Zhang, C. et al. (2006) Structural characterization of autoinhibited c-Met kinase produced by coexpression in bacteria with phosphatase. *Proc. Natl. Acad. Sci. U.S.A.* **103**, 3563–3568 <https://doi.org/10.1073/pnas.0600048103> PMID: 16537444
- 18 Rickert, K.W., Patel, S.B., Allison, T.J., Byrne, N.J., Darke, P.L., Ford, R.E. et al. (2011) Structural basis for selective small molecule kinase inhibition of activated c-Met. *J. Biol. Chem.* **286**, 11218–11225 <https://doi.org/10.1074/jbc.M110.204404> PMID: 21247903
- 19 Jura, N., Zhang, X., Endres, N.F., Seeliger, M.A., Schindler, T. and Kuriyan, J. (2011) Catalytic control in the EGF receptor and its connection to general kinase regulatory mechanisms. *Mol. Cell* **42**, 9–22 <https://doi.org/10.1016/j.molcel.2011.03.004> PMID: 21474065
- 20 Huse, M. and Kuriyan, J. (2002) The conformational plasticity of protein kinases. *Cell* **109**, 275–282 [https://doi.org/10.1016/S0092-8674\(02\)00741-9](https://doi.org/10.1016/S0092-8674(02)00741-9) PMID: 12015977

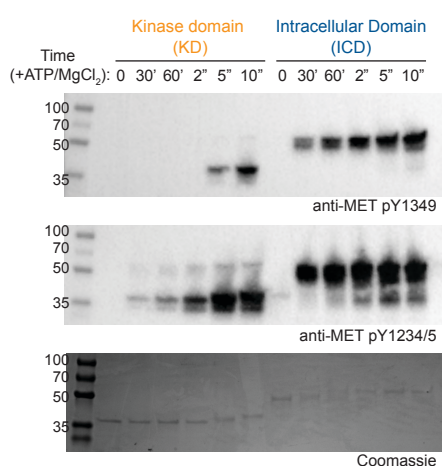
- 21 Michieli, P., Basilio, C., Pennacchietti, S., Maffè, A., Tamagnone, L., Giordano, S. et al. (1999) Mutant Met-mediated transformation is ligand-dependent and can be inhibited by HGF antagonists. *Oncogene* **18**, 5221–5231 <https://doi.org/10.1038/sj.onc.1202899> PMID: 10498872
- 22 Jeffers, M.F. and Vande Woude, G.F. (1999) Activating mutations in the Met receptor overcome the requirement for autophosphorylation of tyrosines crucial for wild type signaling. *Oncogene* **18**, 5120–5125 <https://doi.org/10.1038/sj.onc.1202902> PMID: 10490849
- 23 Jeffers, M., Schmidt, L., Nakaigawa, N., Webb, C.P., Weirich, G., Kishida, T. et al. (1997) Activating mutations for the met tyrosine kinase receptor in human cancer. *Proc. Natl. Acad. Sci. U.S.A.* **94**, 11445–11450 <https://doi.org/10.1073/pnas.94.21.11445> PMID: 9326629
- 24 Guérin, C. and Tulasne, D. (2024) Recording and classifying MET receptor mutations in cancers. *Elife* **13**, e92762 <https://doi.org/10.7554/eLife.92762> PMID: 38652103
- 25 Timofeevski, S.L., McTigue, M.A., Ryan, K., Cui, J., Zou, H.Y., Zhu, J.X. et al. (2009) Enzymatic characterization of c-Met receptor tyrosine kinase oncogenic mutants and kinetic studies with aminopyridine and triazolopyrazine inhibitors. *Biochemistry* **48**, 5339–5349 <https://doi.org/10.1021/bi900438w> PMID: 19459657
- 26 Ma, P.C., Kijima, T., Maulik, G., Fox, E.A., Sattler, M., Griffin, J.D. et al. (2003) c-MET mutational analysis in small cell lung cancer: novel juxtamembrane domain mutations regulating cytoskeletal functions. *Cancer Res.* **63**, 6272–6281 PMID: 14559814
- 27 Cancer Genome Atlas Research N. (2014) Cancer genome atlas research n. comprehensive molecular profiling of lung adenocarcinoma. *Nature* **511**, 543–550 <https://doi.org/10.1038/nature13385>
- 28 Kong-Beltran, M., Seshagiri, S., Zha, J., Zhu, W., Bhawe, K., Mendoza, N. et al. (2006) Somatic mutations lead to an oncogenic deletion of met in lung cancer. *Cancer Res.* **66**, 283–289 <https://doi.org/10.1158/0008-5472.CAN-05-2749> PMID: 16397241
- 29 Frampton, G.M., Ali, S.M., Rosenzweig, M., Chmielecki, J., Lu, X., Bauer, T.M. et al. (2015) Activation of MET via diverse exon 14 splicing alterations occurs in multiple tumor types and confers clinical sensitivity to MET inhibitors. *Cancer Discov.* **5**, 850–859 <https://doi.org/10.1158/2159-8290.CD-15-0285> PMID: 25971938
- 30 Hubbard, S.R. (2004) Juxtamembrane autoinhibition in receptor tyrosine kinases. *Nat. Rev. Mol. Cell Biol.* **5**, 464–471 <https://doi.org/10.1038/nrm1399> PMID: 15173825
- 31 Irueta, P.M., Luo, Y., Bakht, O., Lai, C.C., Smith, S.O. and DiMaio, D. (2002) Definition of an inhibitory juxtamembrane WW-like domain in the platelet-derived growth factor beta receptor. *J. Biol. Chem.* **277**, 38627–38634 <https://doi.org/10.1074/jbc.M204890200> PMID: 12181311
- 32 Wybenga-Groot, L.E., Baskin, B., Ong, S.H., Tong, J., Pawson, T. and Sicheri, F. (2001) Structural basis for autoinhibition of the Ephb2 receptor tyrosine kinase by the unphosphorylated juxtamembrane region. *Cell* **106**, 745–757 [https://doi.org/10.1016/S0092-8674\(01\)00496-2](https://doi.org/10.1016/S0092-8674(01)00496-2) PMID: 11572780
- 33 Mol, C.D., Dougan, D.R., Schneider, T.R., Skene, R.J., Kraus, M.L., Scheibe, D.N. et al. (2004) Structural Basis for the Autoinhibition and STI-571 Inhibition of c-Kit Tyrosine Kinase. *Journal of Biological Chemistry* **279**, 31655–31663 <https://doi.org/10.1074/jbc.M403319200>
- 34 Griffith, J., Black, J., Faerman, C., Swenson, L., Wynn, M., Lu, F. et al. (2004) The structural basis for autoinhibition of FLT3 by the juxtamembrane domain. *Mol. Cell* **13**, 169–178 [https://doi.org/10.1016/S1097-2765\(03\)00505-7](https://doi.org/10.1016/S1097-2765(03)00505-7) PMID: 14759363
- 35 Zhang, X., Gureasko, J., Shen, K., Cole, P.A. and Kuriyan, J. (2006) An allosteric mechanism for activation of the kinase domain of epidermal growth factor receptor. *Cell* **125**, 1137–1149 <https://doi.org/10.1016/j.cell.2006.05.013> PMID: 16777603
- 36 Jura, N., Endres, N.F., Engel, K., Deindl, S., Das, R., Lamers, M.H. et al. (2009) Mechanism for activation of the EGF receptor catalytic domain by the juxtamembrane segment. *Cell* **137**, 1293–1307 <https://doi.org/10.1016/j.cell.2009.04.025> PMID: 19563760
- 37 Craddock, B.P., Cotter, C. and Miller, W.T. (2007) Autoinhibition of the insulin-like growth factor I receptor by the juxtamembrane region. *FEBS Lett.* **581**, 3235–3240 <https://doi.org/10.1016/j.febslet.2007.06.014>
- 38 Li, S., Covino, N.D., Stein, E.G., Till, J.H. and Hubbard, S.R. (2003) Structural and Biochemical Evidence for an Autoinhibitory Role for Tyrosine 984 in the Juxtamembrane Region of the Insulin Receptor. *Journal of Biological Chemistry* **278**, 26007–26014 <https://doi.org/10.1074/jbc.M302425200>
- 39 Cabail, M.Z., Li, S., Lemmon, E., Bowen, M.E., Hubbard, S.R. and Miller, W.T. (2015) The insulin and IGF1 receptor kinase domains are functional dimers in the activated state. *Nat. Commun.* **6**, 6406 <https://doi.org/10.1038/ncomms7406> PMID: 25758790
- 40 Peschard, P., Fournier, T.M., Lamorte, L., Naujokas, M.A., Band, H., Langdon, W.Y. et al. (2001) Mutation of the c-Cbl TKB domain binding site on the Met receptor tyrosine kinase converts it into a transforming protein. *Mol. Cell* **8**, 995–1004 [https://doi.org/10.1016/S1097-2765\(01\)00378-1](https://doi.org/10.1016/S1097-2765(01)00378-1) PMID: 11741535
- 41 Abella, J.V., Peschard, P., Naujokas, M.A., Lin, T., Saucier, C., Urbé, S. et al. (2005) Met/Hepatocyte growth factor receptor ubiquitination suppresses transformation and is required for Hrs phosphorylation. *Mol. Cell. Biol.* **25**, 9632–9645 <https://doi.org/10.1128/MCB.25.21.9632-9645.2005> PMID: 16227611
- 42 Hashigasako, A., Machide, M., Nakamura, T., Matsumoto, K. and Nakamura, T. (2004) Bi-directional regulation of Ser-985 phosphorylation of c-met via protein kinase C and protein phosphatase 2A involves c-Met activation and cellular responsiveness to hepatocyte growth factor. *J. Biol. Chem.* **279**, 26445–26452 <https://doi.org/10.1074/jbc.M314254200> PMID: 15075332
- 43 Gandino, L., Longati, P., Medico, E., Prat, M. and Comoglio, P.M. (1994) Phosphorylation of serine 985 negatively regulates the hepatocyte growth factor receptor kinase. *J. Biol. Chem.* **269**, 1815–1820 PMID: 8294430
- 44 Tulasne, D., Deheuninck, J., Lourenco, F.C., Lamballe, F., Ji, Z., Leroy, C. et al. (2004) Proapoptotic function of the MET tyrosine kinase receptor through caspase cleavage. *Mol. Cell. Biol.* **24**, 10328–10339 <https://doi.org/10.1128/MCB.24.23.10328-10339.2004> PMID: 15542841
- 45 Duplaquet, L., Leroy, C., Vincent, A., Paget, S., Lefebvre, J., Vanden Abeele, F. et al. (2020) Control of cell death/survival balance by the MET dependence receptor. *Elife* **9**, e50041 <https://doi.org/10.7554/eLife.50041> PMID: 32091387
- 46 Foveau, B., Leroy, C., Ancot, F., Deheuninck, J., Ji, Z., Fafeur, V. et al. (2007) Amplification of apoptosis through sequential caspase cleavage of the MET tyrosine kinase receptor. *Cell Death Differ.* **14**, 752–764 <https://doi.org/10.1038/sj.cdd.4402080> PMID: 17186028
- 47 Fernandes, M., Paget, S., Kherrouche, Z., Truong, M.-J., Vincent, A., Meneboo, J.-P. et al. (2023) Transforming properties of MET receptor exon 14 skipping can be recapitulated by loss of the CBL ubiquitin ligase binding site. *FEBS Lett.* **597**, 2301–2315 <https://doi.org/10.1002/1873-3468.14702> PMID: 37468447

- 48 Barker, S.C., Kassel, D.B., Weigl, D., Huang, X., Luther, M.A. and Knight, W.B. (1995) Characterization of pp60c-src tyrosine kinase activities using a continuous assay: autoactivation of the enzyme is an intermolecular autophosphorylation process. *Biochemistry* **34**, 14843–14851 <https://doi.org/10.1021/bi00045a027> PMID: 7578094
- 49 Eathiraj, S., Palma, R., Volckova, E., Hirschi, M., France, D.S., Ashwell, M.A. et al. (2011) Discovery of a novel mode of protein kinase inhibition characterized by the mechanism of inhibition of human mesenchymal-epithelial transition factor (c-Met) protein autophosphorylation by ARQ 197. *J. Biol. Chem.* **286**, 20666–20676 <https://doi.org/10.1074/jbc.M110.213801> PMID: 21454604
- 50 Bardelli, A., Longati, P., Williams, T.A., Benvenuti, S. and Comoglio, P.M. (1999) A peptide representing the carboxyl-terminal tail of the met receptor inhibits kinase activity and invasive growth. *J. Biol. Chem.* **274**, 29274–29281 <https://doi.org/10.1074/jbc.274.41.29274> PMID: 10506185
- 51 Gual, P., Giordano, S., Anguissola, S. and Comoglio, P.M. (2001) Differential requirement of the last C-terminal tail of Met receptor for cell transformation and invasiveness. *Oncogene* **20**, 5493–5502 <https://doi.org/10.1038/sj.onc.1204713> PMID: 11571647
- 52 Estevam, G.O., Linossi, E.M., Macdonald, C.B., Espinoza, C.A., Michaud, J.M., Coyote-Maestas, W. et al. (2024) Conserved regulatory motifs in the juxtamembrane domain and kinase N-lobe revealed through deep mutational scanning of the MET receptor tyrosine kinase domain. *Elife* **12**, RP91619 <https://doi.org/10.7554/eLife.91619> PMID: 39268701
- 53 Hedger, G., Sansom, M.S.P. and Koldsø, H. (2015) The juxtamembrane regions of human receptor tyrosine kinases exhibit conserved interaction sites with anionic lipids. *Sci. Rep.* **5**, 9198 <https://doi.org/10.1038/srep09198> PMID: 25779975
- 54 Chang, K.T., Guo, J., Di Ronza, A. and Sardiello, M. (2018) Aminode: identification of evolutionary constraints in the human proteome. *Sci. Rep.* **8**, 1357 <https://doi.org/10.1038/s41598-018-19744-w>
- 55 Hornbeck, P.V., Zhang, B., Murray, B., Kornhauser, J.M., Latham, V. and Skrzypek, E. (2015) PhosphoSitePlus, 2014: mutations, PTMs and recalibrations. *Nucleic Acids Res.* **43**, D512–20 <https://doi.org/10.1093/nar/gku1267> PMID: 25514926
- 56 Drozdetskiy, A., Cole, C., Procter, J. and Barton, G.J. (2015) JPred4: a protein secondary structure prediction server. *Nucleic Acids Res.* **43**, W389–94 <https://doi.org/10.1093/nar/gkv332> PMID: 25883141
- 57 Abramson, J., Adler, J., Dunger, J., Evans, R., Green, T., Pritzel, A. et al. (2024) Accurate structure prediction of biomolecular interactions with AlphaFold 3. *Nature* **630**, 493–500 <https://doi.org/10.1038/s41586-024-07487-w> PMID: 38718835
- 58 Park, M., Dean, M., Cooper, C.S., Schmidt, M., O'Brien, S.J., Blair, D.G. et al. (1986) Mechanism of met oncogene activation. *Cell* **45**, 895–904 [https://doi.org/10.1016/0092-8674\(86\)90564-7](https://doi.org/10.1016/0092-8674(86)90564-7) PMID: 2423252
- 59 Hays, J.L. and Watowich, S.J. (2003) Oligomerization-induced modulation of TPR-MET tyrosine kinase activity. *J. Biol. Chem.* **278**, 27456–27463 <https://doi.org/10.1074/jbc.M210648200> PMID: 12711601
- 60 Saucier, C., Papavasiliou, V., Palazzo, A., Naujokas, M.A., Kremer, R. and Park, M. (2002) Use of signal specific receptor tyrosine kinase oncoproteins reveals that pathways downstream from Grb2 or Shc are sufficient for cell transformation and metastasis. *Oncogene* **21**, 1800–1811 <https://doi.org/10.1038/sj.onc.1205261> PMID: 11896612
- 61 Vigna, E., Gramaglia, D., Longati, P., Bardelli, A. and Comoglio, P.M. (1999) Loss of the exon encoding the juxtamembrane domain is essential for the oncogenic activation of TPR-MET. *Oncogene* **18**, 4275–4281 <https://doi.org/10.1038/sj.onc.1202791> PMID: 10435641
- 62 Peschard, P. and Park, M. (2007) From Tpr-Met to Met, tumorigenesis and tubes. *Oncogene* **26**, 1276–1285 <https://doi.org/10.1038/sj.onc.1210201> PMID: 17322912
- 63 Wei, X., Hao, L., Ni, S., Liu, Q., Xu, J. and Correll, P.H. (2005) Altered exon usage in the juxtamembrane domain of mouse and human RON regulates receptor activity and signaling specificity. *J. Biol. Chem.* **280**, 40241–40251 <https://doi.org/10.1074/jbc.M506806200> PMID: 16166096
- 64 Wang, X., Yennawar, N. and Hankey, P.A. (2014) Autoinhibition of the Ron receptor tyrosine kinase by the juxtamembrane domain. *Cell Commun. Signal* **12**, 28 <https://doi.org/10.1186/1478-811X-12-28> PMID: 24739671
- 65 Johnson, J.D., Edman, J.C. and Rutter, W.J. (1993) A receptor tyrosine kinase found in breast carcinoma cells has an extracellular discoidin I-like domain. *Proc. Natl. Acad. Sci. U.S.A.* **90**, 5677–5681 <https://doi.org/10.1073/pnas.90.12.5677> PMID: 8390675
- 66 Agarwal, G., Smith, A.W. and Jones, B. (2019) Discoidin domain receptors: Micro insights into macro assemblies. *Biochim. Biophys. Acta Mol. Cell Res* **1866**, 118496 <https://doi.org/10.1016/j.bbamcr.2019.06.010> PMID: 31229648
- 67 Guérin, C., Vincent, A., Fernandes, M., Damour, I., Laratte, A., Tellier, R. et al. (2025) MET variants with activating N-lobe mutations identified in hereditary papillary renal cell carcinomas still require ligand stimulation. *Mol. Oncol.* **19**, 2366–2387 <https://doi.org/10.1002/1878-0261.13806> PMID: 39980226
- 68 Fernandes, M., Hoggard, B., Jamme, P., Paget, S., Truong, M.-J., Grégoire, V. et al. (2023) MET exon 14 skipping mutation is a hepatocyte growth factor (HGF)-dependent oncogenic driver in vitro and in humanised HGF knock-in mice. *Mol. Oncol.* **17**, 2257–2274 <https://doi.org/10.1002/1878-0261.13397> PMID: 36799689
- 69 Lock, L.S., Frigault, M.M., Saucier, C. and Park, M. (2003) Grb2-independent recruitment of Gab1 requires the C-terminal lobe and structural integrity of the Met receptor kinase domain. *J. Biol. Chem.* **278**, 30083–30090 <https://doi.org/10.1074/jbc.M302675200> PMID: 12766170
- 70 Yokoyama, N., Ischenko, I., Hayman, M.J. and Miller, W.T. (2005) The C terminus of RON tyrosine kinase plays an autoinhibitory role. *J. Biol. Chem.* **280**, 8893–8900 <https://doi.org/10.1074/jbc.M412623200> PMID: 15632155
- 71 Bahcall, M., Sim, T., Paweletz, C.P., Patel, J.D., Alden, R.S., Kuang, Y. et al. (2016) Acquired METD1228V Mutation and Resistance to MET Inhibition in Lung Cancer. *Cancer Discov.* **6**, 1334–1341 <https://doi.org/10.1158/2159-8290.CD-16-0686> PMID: 27694386
- 72 Dong, H.J., Li, P., Wu, C.L., Zhou, X.Y., Lu, H.J. and Zhou, T. (2016) Response and acquired resistance to crizotinib in Chinese patients with lung adenocarcinomas harboring MET Exon 14 splicing alternations. *Lung Cancer (Auckl)*. **102**, 118–121 <https://doi.org/10.1016/j.lungcan.2016.11.006>
- 73 Jin, W., Shan, B., Liu, H., Zhou, S., Li, W., Pan, J. et al. (2019) Acquired Mechanism of Crizotinib Resistance in NSCLC with MET Exon 14 Skipping. *J. Thorac. Oncol.* **14**, e137–e139 <https://doi.org/10.1016/j.jtho.2019.04.021>
- 74 Li, A., Yang, J., Zhang, X., Zhang, Z., Su, J., Gou, L. et al. (2017) Acquired MET Y1248H and D1246N Mutations Mediate Resistance to MET Inhibitors in Non-Small Cell Lung Cancer. *Clin. Cancer Res.* **23**, 4929–4937 <https://doi.org/10.1158/1078-0432.CCR-16-3273>
- 75 Recondo, G., Bahcall, M., Spurr, L.F., Che, J., Ricciuti, B., Leonardi, G.C. et al. (2020) Molecular Mechanisms of Acquired Resistance to MET Tyrosine Kinase Inhibitors in Patients with MET Exon 14-Mutant NSCLC. *Clin. Cancer Res.* **26**, 2615–2625 <https://doi.org/10.1158/1078-0432.CCR-19-3608> PMID: 32034073

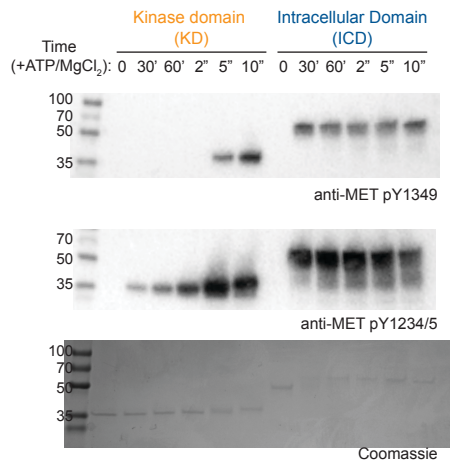
- 76 Sievers, F., Wilm, A., Dineen, D., Gibson, T.J., Karplus, K., Li, W. et al. (2011) Fast, scalable generation of high-quality protein multiple sequence alignments using Clustal Omega. *Mol. Syst. Biol.* **7**, 539 <https://doi.org/10.1038/msb.2011.75> PMID: 21988835
- 77 Mészáros, B., Erdos, G. and Dosztányi, Z. (2018) IUPred2A: context-dependent prediction of protein disorder as a function of redox state and protein binding. *Nucleic Acids Res.* **46**, W329–W337 <https://doi.org/10.1093/nar/gky384> PMID: 29860432

# Supplementary Data 1

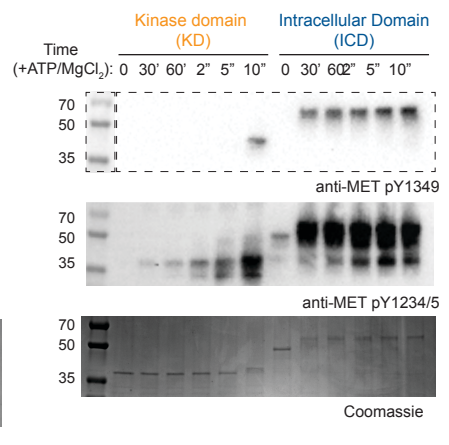
Linossi et al



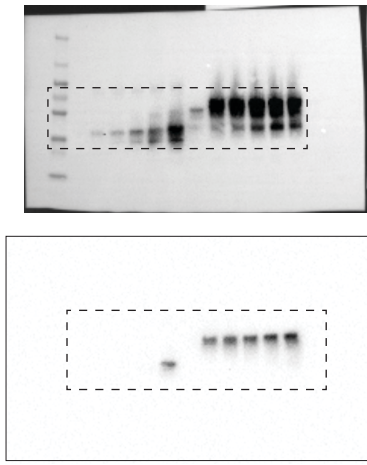
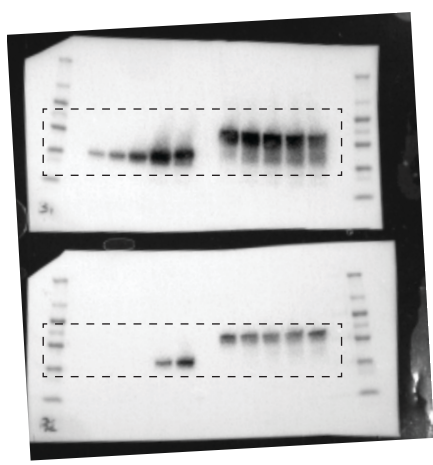
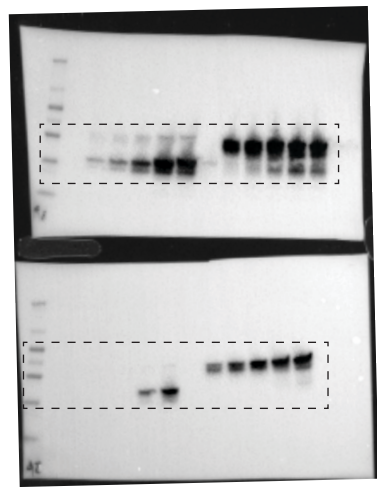
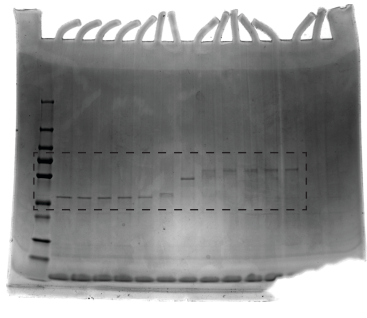
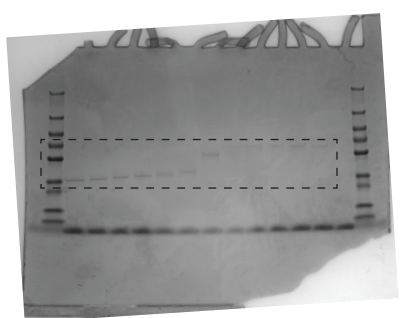
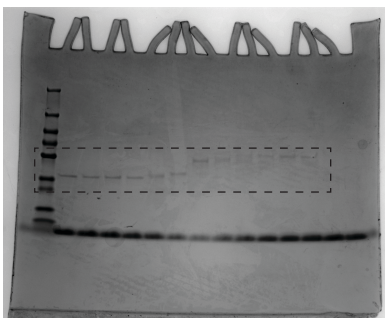
Experiment A  
(Figure 1D)



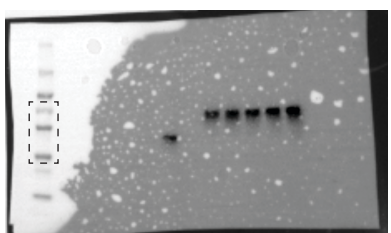
Experiment B



Experiment C



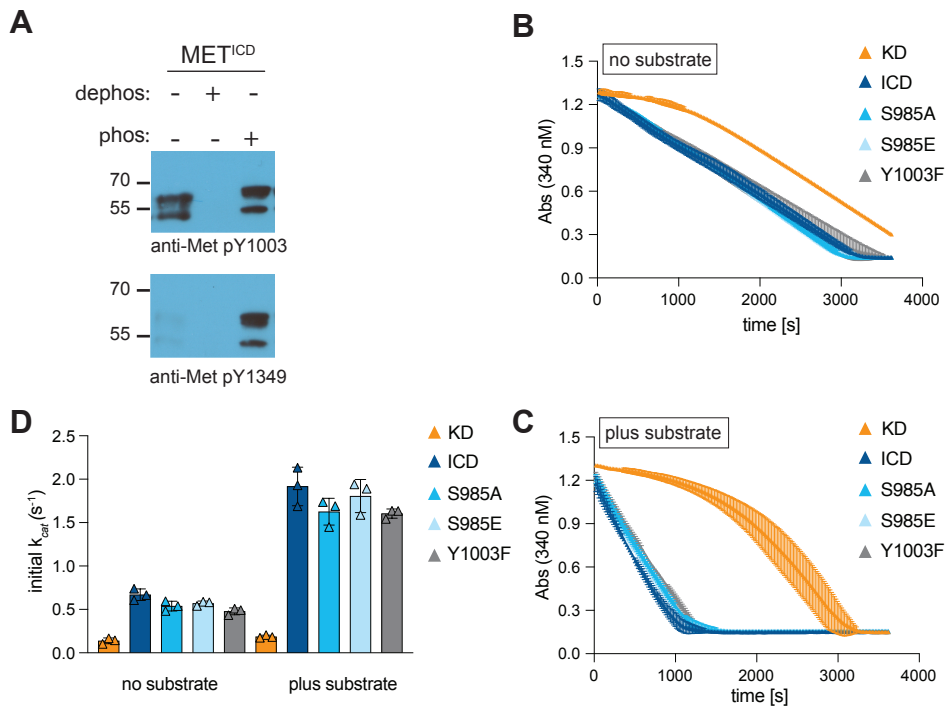
Chemiluminescence image for Experiment C  
Boxed area represents region used for Experiment C image  
See image below for blot dimensions and edges



Colorimetric image for molecular weight ladder overlay for Experiment C  
Boxed area represents region used for Experiment C image

# Supplementary Figure 3

Linossi et al



| Protein                                  | Autophosphorylation              |    |                       |                       | Substrate dependent                        |    |                 |                       |
|--|----------------------------------|----|-----------------------|-----------------------|--|----|-----------------|-----------------------|
|  | $k_{cat}$ ( $S^{-1}$ ) $\pm$ SEM | n= | p (vs KD)             | p (vs ICD)            | $k_{cat}$ ( $S^{-1}$ ) $\pm$ SEM $\pm$ SEM | n= | p (vs KD)       | p (vs ICD)            |
| KD                                       | 0.104 $\pm$ 0.023                | 9  | -                     | <0.0001               | 0.168 $\pm$ 0.019                          | 9  | -               | <0.0001               |
| ICD                                      | 0.466 $\pm$ 0.036                | 9  | <0.0001               | -                     | 1.546 $\pm$ 0.172                          | 9  | <0.0001         | -                     |
| KD <sup><math>\Delta</math>C-tail</sup>  | 0.052 $\pm$ 0.017                | 3  | ns                    | -                     | 0.167 $\pm$ 0.033                          | 3  | ns              | -                     |
| ICD <sup><math>\Delta</math>C-tail</sup> | 0.394 $\pm$ 0.091                | 2  | -                     | ns                    | 2.707 $\pm$ 0.122                          | 2  | -               | 0.0015                |
| ICD <sup><math>\Delta</math>JM1</sup>    | 0.055 $\pm$ 0.013                | 5  | ns                    | <0.0001               | 0.131 $\pm$ 0.030                          | 3  | ns              | <0.0001               |
| ICD <sup><math>\Delta</math>JM2</sup>    | 0.268 $\pm$ 0.065                | 3  | ns                    | ns                    | 2.021 $\pm$ 0.088                          | 2  | 0.0234          | 0.0381                |
| ICD <sup>JM2=GSL</sup>                   | 0.680 $\pm$ 0.079                | 2  | ns                    | ns                    | 1.833 $\pm$ 1.074                          | 2  | ns              | ns                    |
| ICD <sup>Y1003F</sup>                    | 0.433 $\pm$ 0.016                | 4  | <0.0001               | ns                    | 1.466 $\pm$ 0.092                          | 4  | 0.0005          | ns                    |
| ICD <sup>S985A</sup>                     | 0.449 $\pm$ 0.038                | 5  | <0.0001               | ns                    | 1.407 $\pm$ 0.231                          | 5  | 0.0057          | ns                    |
| ICD <sup>S985E</sup>                     | 0.470 $\pm$ 0.058                | 3  | 0.0137                | ns                    | 1.571 $\pm$ 0.153                          | 3  | 0.0107          | ns                    |
| TPR-MET                                  | 0.147 $\pm$ 0.025                | 2  | ns                    | 0.0163                | 0.294 $\pm$ 0.082                          | 2  | ns              | 0.0016                |
| TPR-MET <sup>+Ex14</sup>                 | 0.267 $\pm$ 0.002                | 2  | ns                    | ns                    | 0.729 $\pm$ 0.143                          | 2  | 0.0459          | 0.0219                |
| KD (phos)                                | 0.944 $\pm$ 0.440                | 3  | -                     | ns <sup>#</sup>       | 3.915 $\pm$ 0.825                          | 3  | -               | ns <sup>#</sup>       |
| ICD (phos)                               | 1.003 $\pm$ 0.366                | 3  | ns <sup>#</sup>       | -                     | 2.895 $\pm$ 0.801                          | 3  | ns <sup>#</sup> | -                     |
| RON <sup>KD</sup>                        | 0.036 $\pm$ 0.004                | 3  | -                     | 0.0052 <sup>###</sup> | 0.076 $\pm$ 0.011                          | 3  | -               | ns                    |
| RON <sup>ICD</sup>                       | 0.069 $\pm$ 0.002                | 3  | 0.0052 <sup>###</sup> | -                     | 0.072 $\pm$ 0.006                          | 3  | ns              | -                     |
| RON <sup><math>\Delta</math>JMB</sup>    | 0.086 $\pm$ 0.018                | 3  | ns                    | ns                    | 0.099 $\pm$ 0.007                          | 3  | ns              | 0.0452 <sup>###</sup> |
| RON <sup>EDE-AAA</sup>                   | 0.083 $\pm$ 0.010                | 3  | 0.0278 <sup>###</sup> | ns                    | 0.145 $\pm$ 0.036                          | 3  | ns              | ns                    |

**Supplementary Table 1. Summary values and statistical analysis from coupled kinase assays.** Average values from independent experimental means and SEM values are shown. Each independent experiment was conducted with at least three technical replicates. p-values were calculated using Welch's t-test on independent experimental means. The autophosphorylation or substrate dependent activity of the MET KD and ICD were compared to all other dephosphorylated MET and TPR-MET constructs. <sup>#</sup>Equivalent statistical tests were performed comparing the activity of the phosphorylated KD and ICD to each other. <sup>###</sup>The activity of the RON KD and ICD were compared to each other and the RON ICD mutants. SEM = standard error of the mean; ns = not significant.

| Protein                  | Autophosphorylation<br>RLU fold-change<br>relative to KD $\pm$ SEM | n= | Substrate dependent<br>RLU fold-change<br>relative to KD $\pm$ SEM | n= |
|--------------------------|--|----|--|----|
| KD                       | 1.00 $\pm$ 0.00  | 2  | 1.11 $\pm$ 0.11  | 2  |
| ICD                      | 2.82 $\pm$ 0.00  | 2  | 2.94 $\pm$ 0.54  | 2  |
| TPR-MET                  | 1.86 $\pm$ 0.30  | 2  | 1.23 $\pm$ 0.50  | 2  |
| TPR-MET <sup>+Ex14</sup> | 2.47 $\pm$ 0.58  | 2  | 2.56 $\pm$ 0.62  | 2  |

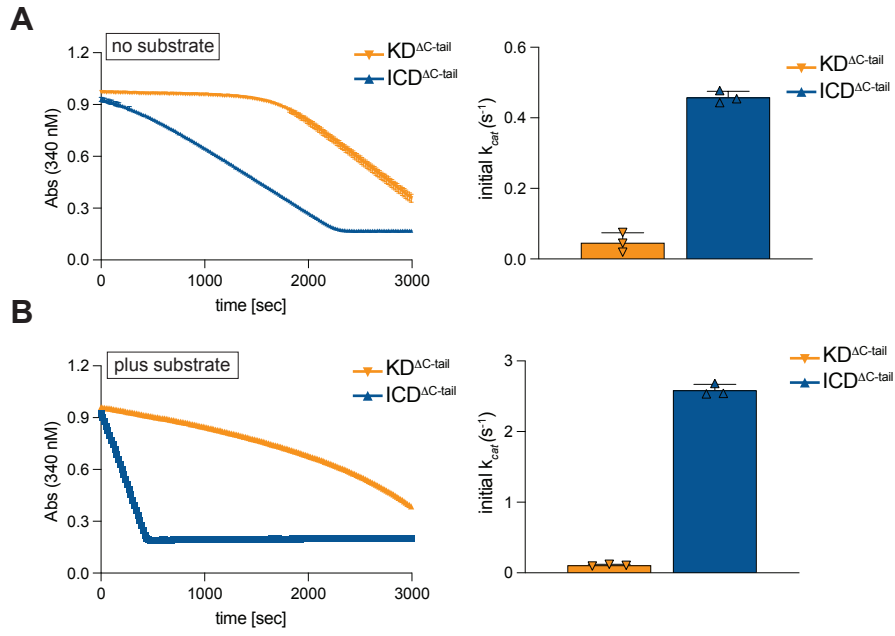
**Supplementary Table 2. Summary values of ADP-Glo assays.** Average values from independent experimental means and SEM values are shown from ADP-Glo assays. Each independent experiment was conducted with at least four technical replicates. SEM = standard error of the mean; RLU = relative luciferase

**Supplementary Table 2. Details of recombinant protein constructs.**

| Protein                  | Construct boundaries         | Description   |
|--------------------------|------------------------------|---|
| KD                       | Q1048-S1390                  | Wildtype MET kinase domain  |
| ICD                      | K956-S1390                   | Wildtype MET full intracellular domain  |
| KD <sup>ΔC-tail</sup>    | Q1048-G1346                  | Wildtype MET kinase domain lacking the C-terminal tail  |
| ICD <sup>ΔC-tail</sup>   | K956 - G1346                 | Wildtype MET full intracellular domain lacking the C-terminal tail  |
| ICD <sup>ΔJM1</sup>      | D1010-S1390                  | Wildtype MET intracellular domain lacking JM1 segment (K963-E1009)  |
| ICD <sup>ΔJM2</sup>      | K956-D1010-Q1048-S1390       | Wildtype MET intracellular domain with deletion of JM2 segment (D1010-L1047)  |
| ICD <sup>JM2=GSL</sup>   | K956-D1010-(GS)-Q1048-S1390  | Wildtype MET intracellular domain with JM2 segment (D1010-L1047) replaced with an equivalent length repeating GS linker of 37 amino acids |
| ICD <sup>Y1003F</sup>    | K956-S1390                   | Full MET intracellular domain with Y1003F mutation  |
| ICD <sup>S985A</sup>     | K956-S1390                   | Full MET intracellular domain with S985A mutation   |
| ICD <sup>S985E</sup>     | K956-S1390                   | Full MET intracellular domain with S985E mutation   |
| TPR-MET                  | TPR(A2-T142)MET(D1010-S1390) | Oncogenic TPR-MET fusion protein  |
| TPR-MET <sup>+Ex14</sup> | TPR(A2-T142) MET(D963-S1390) | Oncogenic TPR-MET fusion protein with addition of D963-E1009 of the MET intracellular domain corresponding the exon 14 coding region      |
| RON <sup>KD</sup>        | R1053-T1400                  | Wildtype RON kinase domain  |
| RON <sup>KD</sup>        | R983-T1400                   | Wildtype RON full intracellular domain  |
| RON <sup>ΔJMB</sup>      | R983-del(P1009-V1035)-T1400  | RON intracellular domain lacking P1009-V1035  |
| RON <sup>EDE-AAA</sup>   | R983-T1400                   | RON intracellular domain with E1044, D1045, E1046 mutated to alanines   |

# Supplementary Figure 1

Linossi et al



# Supplementary Figure 2

Linossi et al

